

Surface Energy Fluxes and Coupled Variability in the Tropics of a Coupled General Circulation Model

R. L. MILLER AND X. JIANG

Department of Applied Physics, Columbia University, New York, New York

(Manuscript received 6 October 1995, in final form 20 December 1995)

ABSTRACT

The effect of wind–evaporative feedbacks upon ENSO, and the coupling of Pacific and Indian Ocean variability, is considered based upon a 110-yr simulation from a coupled ocean and atmosphere general circulation model.

ENSO-like modes, which propagate westward, are found in the model Pacific Ocean. Examination of the SST budget shows that the modes amplify and propagate as a result of changes in the surface energy flux and upwelling rates. Surface flux variability is dominated by the solar and evaporative components, and wind–evaporative feedbacks are shown to lead to growth and westward propagation of coupled anomalies in the model Pacific, a region of mean easterly winds. Eastward propagating coupled modes in the model Indian Ocean, a region of mean equatorial westerlies, are also found and are attributed to the same feedback.

Interaction of the Pacific and Indian Ocean modes through the evaporation field is demonstrated, and their relevance to observed coupled ocean–atmosphere variability is considered.

1. Introduction

Despite intense solar heating of the Tropics, a local minimum of SST exists in the equatorial Pacific east of the date line. Here, cold water rises to the surface in response to easterly winds, offsetting heating by the absorption of sunlight. Every few years, the winds slacken and the surface waters warm. Rainfall patterns are displaced toward the newly warmed water, and the atmospheric circulation over the entire Pacific is altered. This interruption of the easterlies is part of a broader change in the tropical and global circulation, referred to generally as El Niño and the Southern Oscillation or ENSO.

Observed ENSO events have been extensively described (e.g., Bjerknes 1969; Wyrki 1975; Rasmusson and Carpenter 1982), and in the past decade much progress has been made toward identifying the underlying physical mechanisms. One tool for gaining understanding is the coupled general circulation model (CGCM). These models are designed to simulate the global properties of the atmosphere and ocean, and not ENSO per se. Nonetheless, certain models (e.g., Philander et al. 1992; Latif et al. 1993) have successfully reproduced generic features of ENSO, such as its observed period and growth rate along with the anomalous fields of

SST, wind, and rainfall. CGCMs as a group have succeeded in producing a much larger range of tropical ocean–atmosphere behavior than observed. Differences in model behavior arise because of variations in resolution and parameterization of physical processes like convection and the atmospheric boundary layer. Presumably, this broader range of behavior in part reflects unrealistic assumptions of the models and failures in simulation. However, departures from observations may indicate that there are potentially realizable modes that have not been recognized in the limited observational record. Neelin et al. (1992) have attempted to summarize equatorial variability in CGCMs by comparing behavior in a variety of coupled models. Not all models were found to exhibit interannual variability arising from coupling between the ocean and atmosphere. Within the remainder, the coupled behavior could be broadly distinguished between “stationary” SST anomalies restricted to the East Pacific (e.g., Philander et al. 1992; Latif et al. 1993) or “propagating” modes traveling westward across the basin (e.g., Meehl 1990; Lau et al. 1992). Both types of behavior can be identified within the observations, although the propagating modes tend to occur in CGCMs where resolution within the equatorial waveguide is insufficient to represent all the physical processes believed to be important to the onset of ENSO events.

CGCMs are designed to simulate global climate, including ENSO variability in the equatorial Pacific and its interactions with other tropical oceans and the extratropics. In addition, CGCMs contain modes of variability and representations of physical processes that

Corresponding author address: Dr. Ron L. Miller, Department of Applied Physics, Columbia University, Armstrong 550, New York, NY 10027.
E-mail: rlm15@columbia.edu

are irrelevant to ENSO. This wealth of variability in CGCMs can obscure the physical mechanisms responsible for the ENSO behavior. Much of our understanding of the physics underlying ENSO has come from simplified conceptual models. The physical paradigms derived from these simpler models are used in turn to diagnose the richer and more complicated ENSO variability in CGCMs. One such "simplified" model has been developed by Zebiak and Cane (1987). Surface winds vary in response to SST anomalies, based upon a Gill (1980) atmospheric model (Zebiak 1982, 1986). The change in wind stress excites anomalous ocean currents and displaces the thermocline, according to a reduced-gravity shallow water model. These anomalies in turn modify the original SST anomaly. This model simulates ENSO variability quite successfully, and because of its relative simplicity, has been used to diagnose the physical mechanisms responsible for ENSO. Battisti (1988) found that warming of the model East Pacific is largely the result of anomalously warm water upwelling to the surface. The change in water temperature at depth can be ascribed to a deepening of the thermocline so that upwelling water originates in the relatively warm layer above this level.

According to Battisti and Hirst (1989) along with Suarez and Schopf (1988) and Schopf and Suarez (1990), deepening of the East Pacific thermocline is part of an instability that results from the interaction of oceanic and atmospheric anomalies. Westerly surface wind anomalies excite oceanic Kelvin waves, which depress the thermocline. Warming of the ocean surface reinforces the westerlies, further exciting the Kelvin waves. The same winds excite Rossby waves, which raise the thermocline along their westward trajectory. These waves reflect off the western boundary and return to the East Pacific. Shoaling of the thermocline by the arriving waves halts the warming and moves the anomaly into its cold or "La Niña" phase. In response to the cold SST, anomalous easterly winds form, again exciting Rossby waves, whose effect this time is to lower the thermocline. This is the "delayed oscillator" scenario, whereby wind anomalies constantly excite Rossby waves which act, upon reflection at the western boundary, to drive the East Pacific anomaly into its opposite phase. This conceptual picture motivates a simple equation describing East Pacific SST (Battisti and Hirst 1989; Schopf and Suarez 1990; Cane et al. 1990), with analytic solutions whose growth rate and duration between events are consistent with the behavior of the full Cane-Zebiak model along with the observations.

More complicated analytic models of ENSO have been developed by Neelin (1991), Jin and Neelin (1993a, 1993b), and Neelin and Jin (1993). These are similar to the Cane-Zebiak model except that the SST anomaly is calculated only at the equator. Upwelling of anomalously warm water is destabilizing in this model (Neelin 1991)—consistent with the models of

Battisti and Hirst (1989) and Schopf and Suarez (1990)—as is warming by a reduction of the upwelling velocity, as hypothesized originally by Bjerknes (1969). Neelin also showed the existence of a so-called "SST mode" of coupled variability, distinct from the delayed-oscillator mechanism found in the Cane-Zebiak model. Propagating anomalies in CGCMs are typically identified with the SST mode, while the anomalies localized in the East and Central Pacific of high-resolution CGCMs are regarded as a manifestation of the delayed oscillator (e.g., Philander et al. 1992).

The Cane-Zebiak and Neelin models demonstrate that tropical interannual variability can arise from changes in the East Pacific upwelling rate or a change in the temperature of the upwelling water associated with a change in thermocline depth. Note that heat input from the atmosphere is not required in these models to force the observed changes in the East Pacific ocean temperature. Surface heat fluxes (by solar and long-wave radiation along with sensible and evaporative fluxes) are parameterized as a single, linear, damping term, tending to restore SST to equilibrium. This is motivated in part by observations of ENSO events. Weare (1983) estimated that surface fluxes cool the ocean during the peak phase of ENSO. However, Weare also found that SST and cooling by surface fluxes are slightly out of phase, so that anomalous surface fluxes contribute to the original warming.

Weare noted that surface flux anomalies during ENSO events are dominated by anomalous evaporation. If the bulk parameterization formula for evaporation is linearized, two contributions to the anomalous evaporation result (assuming constant relative humidity). The first arises from perturbations to the equilibrium SST and has the form of Newtonian cooling used to parameterize surface heating in the above models. A second contribution results from changes in the wind stress.

The effect of this evaporation-wind feedback has been previously considered in models of atmospheric equatorial waves (e.g., Neelin et al. 1987; Emanuel 1987; Xie et al. 1993), along with models of the East Pacific ITCZ (Xie and Philander 1994). Strengthening of the total wind increases the rate of evaporation and augments the moisture available for latent heating by deep convection. Increased evaporation also acts to cool the underlying ocean. In the Central Pacific, a region of mean easterlies, anomalous convergence strengthens the *total* surface flow to the east of the convergence and weakens winds to the west. This leads to increased evaporation and cooling of SST to the east and decreased evaporation and warming to the west, which neglecting other effects favors westward displacement of the convergence anomaly. In a simulation of observed Pacific interannual variability, Seager (1989) found that a reduction of wind stress in the Central Pacific during the warming stage of ENSO led to reduced evaporation and anomalous surface heating

that was comparable to the warming by advective processes. His simulation was based upon the Cane–Zebiak model but with surface fluxes computed using bulk parameterizations (including a wind feedback) rather than a Newtonian cooling term. Wind–evaporative feedbacks may account for the out of phase relationship between surface heating and SST found by Weare (1983).

In this article, we describe equatorial interannual variability in a CGCM that results from the interaction of oceanic and atmospheric anomalies. Our goal is to examine the role of surface heat fluxes, especially evaporation, in creating this variability. We will describe how wind–evaporative feedbacks amplify and cause the propagation of anomalies of equatorial SST. Finally, we will show how coupled anomalies originating in the model Pacific excite evaporative anomalies in the Indian Ocean and effectively couple SST variability in the two ocean basins.

In section 2, we describe the coupled model and compare the model's tropical climate to that of observations. In section 3, a coupled mode of interannual variability is described and the SST budget is examined in order to identify the underlying physical processes. The effect of surface heat fluxes and evaporation is examined in section 4, where we also show how surface heating couples the variability in the model Pacific and Indian Oceans. Speculations regarding the role of evaporative anomalies in the observed tropical climate and our conclusions are presented in section 5.

2. The coupled model

a. Model description

The CGCM consists of the NASA/GISS atmospheric GCM, along with an ocean GCM based upon the Bryan–Cox GFDL model (Bryan 1969; Bryan and Cox 1972; Cox 1984).

The AGCM is an improved version of the Model II GCM developed at NASA/GISS (Hansen et al. 1983). Model II has been used for transient greenhouse experiments (Hansen et al. 1988) and simulations of unforced decadal variability (e.g., Barnett et al. 1992; Miller and DelGenio 1994).

Improvements to the parameterizations have resulted in Model II'. A new convective parameterization computes the cumulus mass flux by relaxing the atmosphere to a neutrally stable state at cloud base in one model-physics time step (DelGenio and Yao 1993). Because the model is not assumed to be always in a state of quasi-equilibrium (e.g., Arakawa and Schubert 1974), but instead relaxes toward this state, the model can be used to predict small shifts in thermodynamic structure, which may be significant for climate change. The new scheme also includes a parameterization of convective downdrafts, which can have important transient impacts on evaporative fluxes by regulating the thermodynamic state of the atmospheric boundary layer.

Cloud liquid water and ice are computed prognostically in Model II' and the computation of cloud optical thickness has been modified to depend upon these quantities (DelGenio et al. 1993). For example, tropical cumulonimbus anvils are linked interactively to the convective mass flux, and are now relatively opaque in the new parameterization. The new cloud parameterization produces realistic variability of maritime cloudiness on diurnal, seasonal, and interannual timescales when run with specified SSTs (DelGenio et al. 1996).

Model II' also includes a more realistic treatment of the boundary layer (G. Hartke 1996, personal communication). Similarity theory is used to predict coefficients of turbulent exchange (which link the ground to the surface air layer) and diffusivities (which link the surface air layer to the ocean model first layer). Turbulent exchange coefficients for heat and moisture are now distinct, and roughness lengths over the ocean are specified as a function of momentum flux and are self-consistent with neutral drag coefficients. Druyan et al. (1995) report that the parameterizations cited above significantly improve the model's response to tropical SST anomalies.

The current version of the GISS AGCM has horizontal resolution of $4^\circ \text{ lat} \times 5^\circ \text{ long}$ with nine vertical levels. GISS participates in the model intercomparison projects FANGIO and AMIP. In the first comparison of models to observations, Model II' was found to be among the five most accurate GCMs worldwide, when the model simulation of seasonal variations of cloud forcing was compared to ERBE measurements (R. Cess 1996, personal communication).

The new parameterizations result in more realistic behavior when the AGCM is coupled to the OGCM described below. When the original Model II AGCM was coupled, the ocean thermohaline circulation collapsed and tropical temperatures were excessively warm. In comparison, the new parameterizations of Model II' restore deepwater formation and result in more realistic tropical temperatures.

The oceanic component of the CGCM consists of the GFDL Bryan–Cox OGCM (Bryan 1969; Bryan and Cox 1972; Cox 1984), along with a thermodynamic sea-ice model (Hansen et al. 1983). Horizontal resolution is $4^\circ \text{ lat} \times 5^\circ \text{ long}$, with 16 layers in the vertical. Surface fluxes modify temperature and salinity within the uppermost layer of 30-m depth. (The subsequent three layers in the upper ocean have thicknesses of 60, 90, and 120 m, respectively.) Heat diffusion is parameterized according to Bryan and Lewis (1979), while horizontal and vertical viscous diffusion are set to $4 \times 10^9 \text{ cm}^2 \text{ s}^{-1}$ and $20 \text{ cm}^2 \text{ s}^{-1}$, respectively. The viscous diffusion coefficients were chosen to give the best simulation of the poleward heat and mass transports. With regard to tropical oceanic variability, the OCGM resolution is considered "low" because neither the equatorial waveguide nor the thermocline are well resolved (cf. Lau et al. 1992).

Initialization of the coupled model is carried out by integrating the AGCM for a decade using as a lower boundary condition the seasonal cycle of SST and sea-ice derived from AMIP. The computed surface winds are then used to force the OGCM, while restoring the sea surface temperature and surface salinity to Levitus (1982) annual-mean values. The ocean tracer time step equals one day, while the dynamics time step equals 1 h, and an integration of 6000×365 time steps is carried out, equivalent to 6000 years for the tracer field. Next, seasonally varying values of sea surface temperature and salinity are used to force the OGCM for an additional 500 years, with the tracer time step reduced to 4 h. At this point, the globally integrated surface energy flux [proportional to the difference between the Levitus (1982) temperature and the first model layer temperature] is less than 0.001 W m^{-2} , and the AGCM and OGCM can be coupled. The models exchange fluxes of heat, freshwater, and momentum every hour. These fluxes are updated four times daily, with the values accumulated over the previous 6 h averaged to form an hourly rate.

The model has been integrated without flux correction to simulate 110 years of climate, forced only by diurnal and annual cycles of solar radiation. Figure 1

shows the temporal evolution of the sea surface temperature and salinity simulated by the model for the NH, SH, and global averages. There is drift in the NH surface salinity, largely a reflection of North Atlantic and North Pacific values. The drift is due mainly to the initial incompatibility of the air-sea fluxes needed to maintain the respective uncoupled AGCM and OGCM equilibria. The increasing salinity in the high-latitude oceans invigorates the meridional overturning, increasing the advection of warm and salty waters from subtropical latitudes. This leads to warming in the high latitudes of these oceans, accounting for the slight rise in global and NH SST during the course of the integration. In comparison, tropical means are stable.

We note that our ocean model has a global domain, in comparison to the higher-resolution models of Philander et al. (1992), where ocean temperature is specified outside of the tropical Pacific, and Latif et al. (1993) where ocean temperature and salinity are restored to Levitus (1982) values poleward of 30° latitude.

b. Model climate

We summarize the tropical climatology of the CGCM with emphasis on features that are related to the

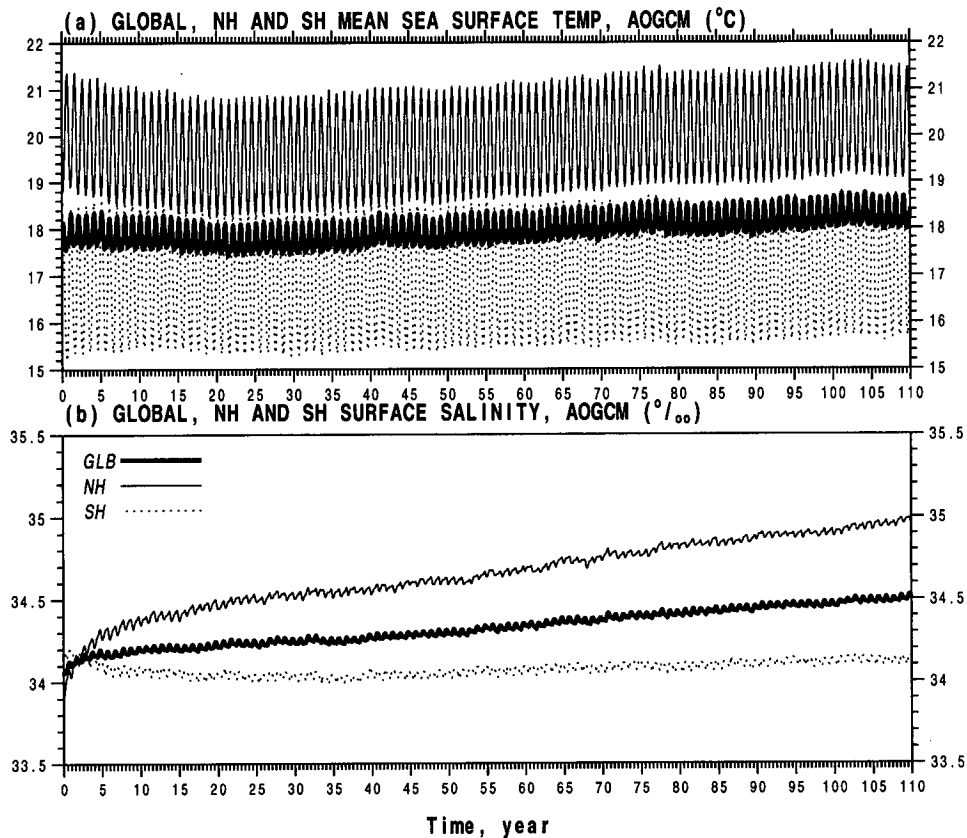


FIG. 1. Global, Northern Hemisphere, and Southern Hemisphere averages of (a) sea surface temperature and (b) salinity.

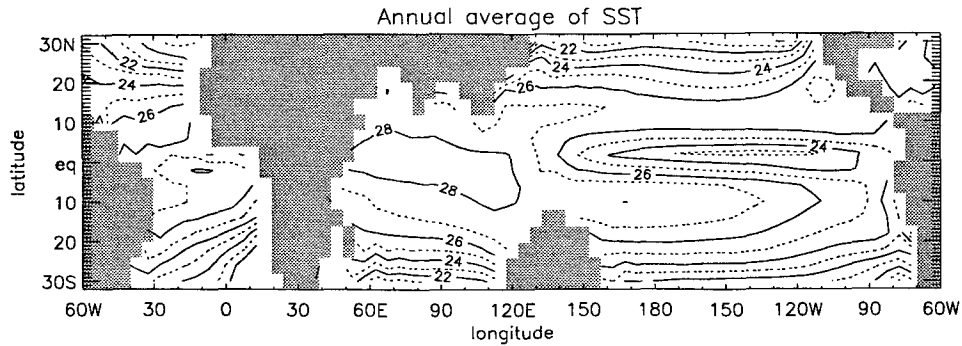


FIG. 2. Annually averaged SST ($^{\circ}\text{C}$) for the first 30 years of the CGCM integration.

interannual variability in the model Pacific and Indian Oceans. All quantities described in this study are derived from the first 30 years of the simulation, although we have found that our conclusions extend to the model behavior during the remaining 80 years as well.

The model SST—that is, temperature in the uppermost ocean layer depth of 30 m—is shown in Fig. 2. Tropical temperatures are relatively uniform in comparison to the steep gradients in midlatitudes. And equatorial temperatures are coldest in the East Pacific, increasing to the west, reaching a broad maximum over the Indian Ocean.

What is noticeably absent is the Pacific warm pool. The zonal extent of the cold tongue is too large in comparison to observations, so that the warm pool is displaced roughly 60° of longitude to the west at the edge of the Indian Ocean. The upwelling zones off the west coasts of Africa and South America are also poorly modeled. Presumably, simulation of these latter features requires high zonal resolution since coastal upwelling appears in simulations using a high-resolution OGCM (Philander and Pacanowski 1981), but not in the CGCMs of Philander et al. (1992) and Latif et al. (1993), which have high meridional resolution concentrated about the equatorial waveguide but comparatively coarse zonal resolution.

The model precipitation field is shown in Fig. 3. Tropical rainfall is coincident with the warmest SST as observed (Zhang 1993). Consequently, departures from observed values of rainfall reflect discrepancies in the model SST fields. Because the cold tongue extends so far west, the SPCZ has a predominantly zonal orientation, forming a double ITCZ. The observed West Pacific rainfall maximum is shifted westward with the warm pool.

The model underestimates observed values of precipitation (Legates and Willmont 1990) by roughly a factor of 2. There is also underestimation of the wind stress field (Fig. 4). Although the general patterns of the low-level wind are realistic, the tropical circulation in the model boundary layer is sluggish in comparison to observations.

Misestimation of the zonal wind stress along the equatorial Pacific is perhaps the result of a coupled instability (Neelin et al. 1992). The easterlies are driven in part by the zonal temperature gradient between the cold tongue and warm pool (Lindzen and Nigam 1987). These winds in turn lead to upwelling as a result of Ekman and geostrophic divergence about the equator (e.g., Stommel 1960). This upwelling will cool the surface more toward the east where the thermocline is shallower resulting in an increased zonal temperature

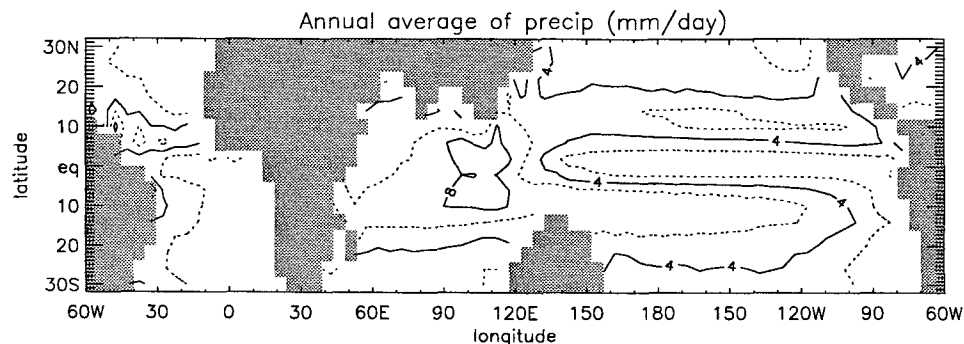


FIG. 3. Annually averaged precipitation (mm day^{-1}).

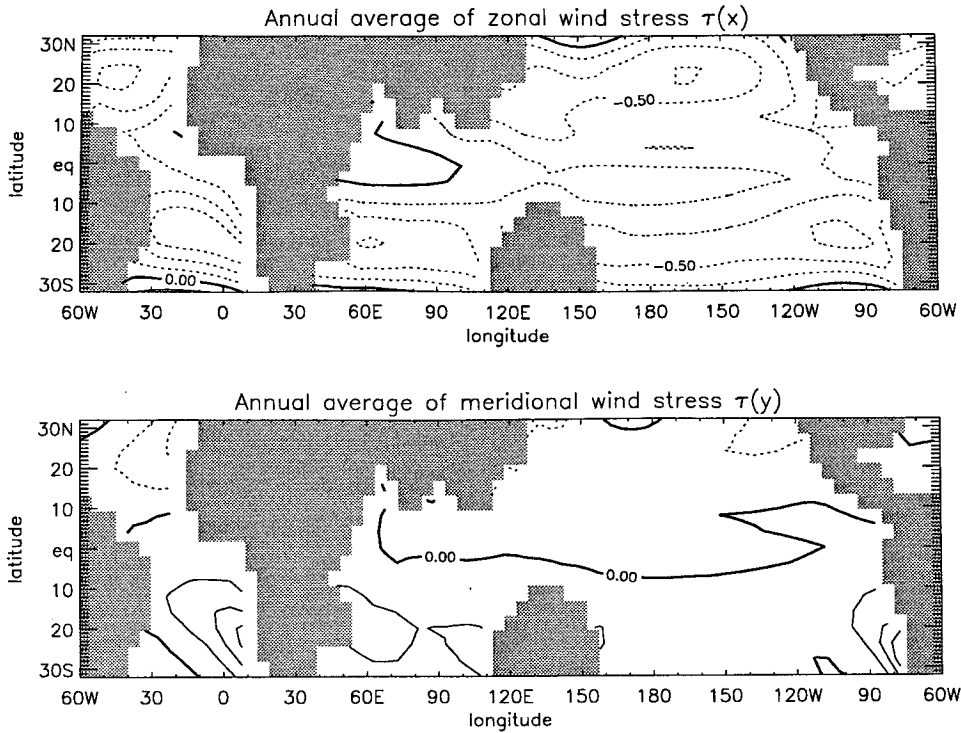


FIG. 4. Annually averaged (a) zonal and (b) meridional wind stress (dynes cm^{-2}).

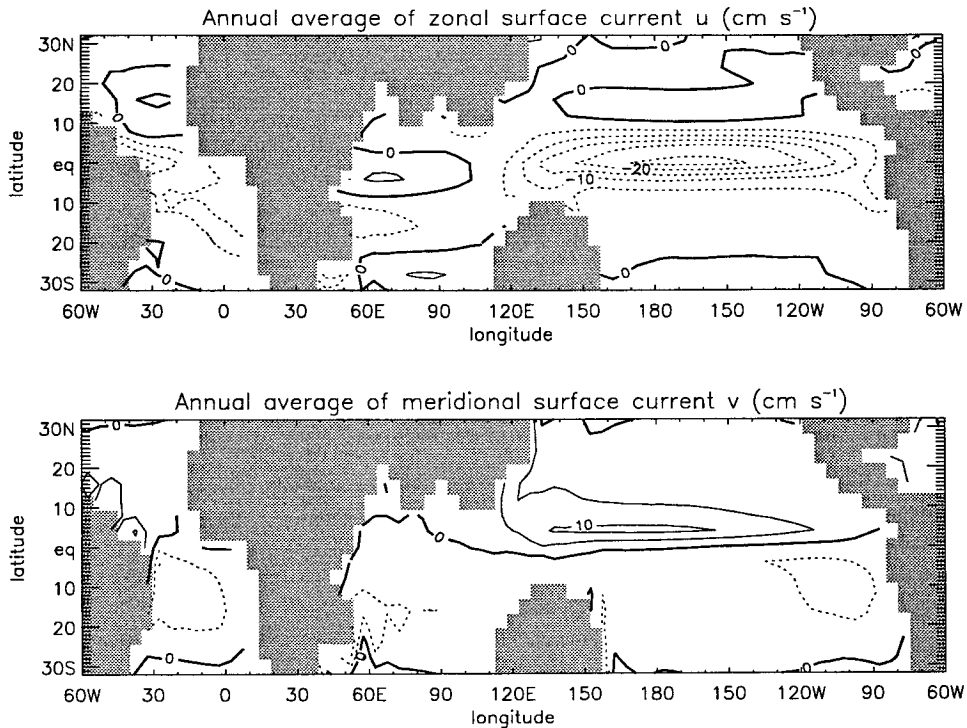


FIG. 5. Annually averaged (a) zonal and (b) meridional surface current (cm s^{-1}).

gradient. [This is essentially the same mechanism that Bjerknes (1969) hypothesized to explain the onset of ENSO.] Thus, models with different sensitivities of surface winds to SST anomalies will find this difference amplified along the equatorial Pacific. Whereas tropical wind stress is underestimated by this model, it is overestimated in the NCAR CGCM (Meehl 1990). While the two models have similar resolution, their parameterizations of moist convection, radiation, and the atmospheric boundary layer—which together determine the surface wind response to SST anomalies—are different.

The surface currents are shown in Fig. 5. Along the equator, flow is downwind and there is divergence of the meridional component, as observed (Philander 1990). A weak North Equatorial Countercurrent extends too far to the north in the Pacific. Like the surface winds, the surface currents are relatively sluggish.

The rate of upwelling into the surface layer—that is, w at 30-m depth—is shown in Fig. 6. The maximum value within the cold tongue of $6 \times 10^{-4} \text{ cm s}^{-1}$ is equivalent to 0.5 m day^{-1} . This is small in comparison to the 1.3 m day^{-1} value estimated at 30-m depth for the East Pacific between 110°W and 150°W (Bryden and Brady 1985). However, this comparison is misleading, since the poor agreement is largely imposed by the model resolution and as such is a generic property of low-resolution OGCMs (cf. Lau et al. 1992). Equatorial upwelling is observed to take place within a latitudinal band that is narrow, compared to the width of a low-resolution model grid box. Because equatorial upwelling is controlled by divergence of the meridional flow—which is largely determined by the magnitude of the easterly wind stress—if the wind stress is similar between observations and the model, then the area-integrated upwelling must be similar as well. Consequently, upwelling in the lower-resolution model must be weaker to compensate for the broader area over which it occurs.

A fairer measure of the simulated upwelling is the product of the vertical velocity and the meridional width over which it occurs. Bryden and Brady (1985)

estimate that the East Pacific upwelling rate of 1.3 m day^{-1} occurs within 1.5° of latitude centered at the equator. From Fig. 6, upwelling in the CGCM is seen to occur over 11° of latitude, with an average velocity of roughly 0.25 m day^{-1} . Thus, the CGCM slightly overestimates the total upward mass flux at 30-m depth, when the differing meridional widths over which upwelling occurs are taken into account. However, while the maximum upwelling rate in the model occurs at 30-m depth, the largest observed value of 2.5 m day^{-1} is found near 60 m (Bryden and Brady 1985). Thus, a comparison of maximum values shows that upwelling in the CGCM peaks closer to the surface and is slightly weaker than observed, consistent with the underestimated equatorial easterlies.

Subsurface fields of ocean temperature and zonal current in the equatorial plane are shown in Figs. 7 and 8, respectively. The isotherms deepen to the west in both the Pacific and Atlantic as observed. However, a comparison to the observed field derived from Levitus (1982) shows that the coupled model is largely lacking a thermocline and instead exhibits a decay of temperature with depth that is unrealistically gradual. This absence of a strong vertical gradient is presumably a consequence of the large diffusion that must be used in such a low-resolution model to mimic the effect of eddies. In comparison, the higher-resolution models (e.g., Philander et al. 1992; Latif et al. 1993) can be integrated with less diffusion and exhibit sharper thermoclines. Presumably, large diffusion—along with the weak easterlies, which cause underestimation of the ocean zonal pressure gradient—is also a reason for the feeble equatorial undercurrent beneath the downwind surface current in Fig. 8.

The weak thermocline may also be responsible for the excessive westward extension of the model's cold tongue and the absence of a Pacific warm pool. The ability of upwelling water to cool the surface is diminished in the West Pacific, because the water begins its ascent at a warmer depth in the west, as a result of the observed zonal tilt of the thermocline. Because this strong zonal gradient of temperature at a fixed depth is

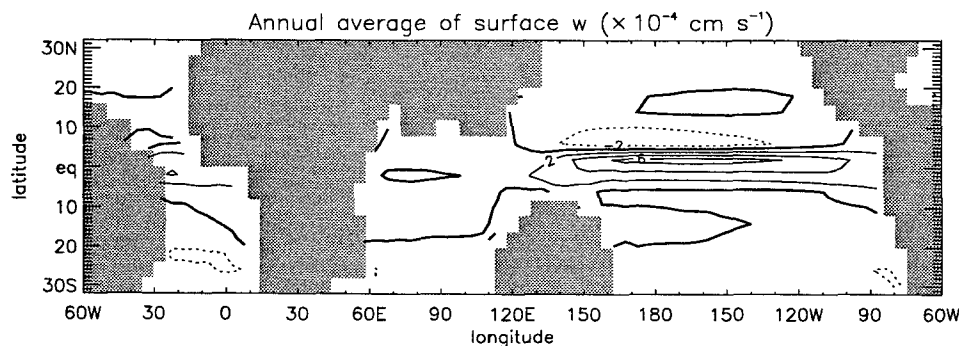


FIG. 6. Annually averaged upwelling into the surface layer ($\times 10^{-4} \text{ cm s}^{-1}$).

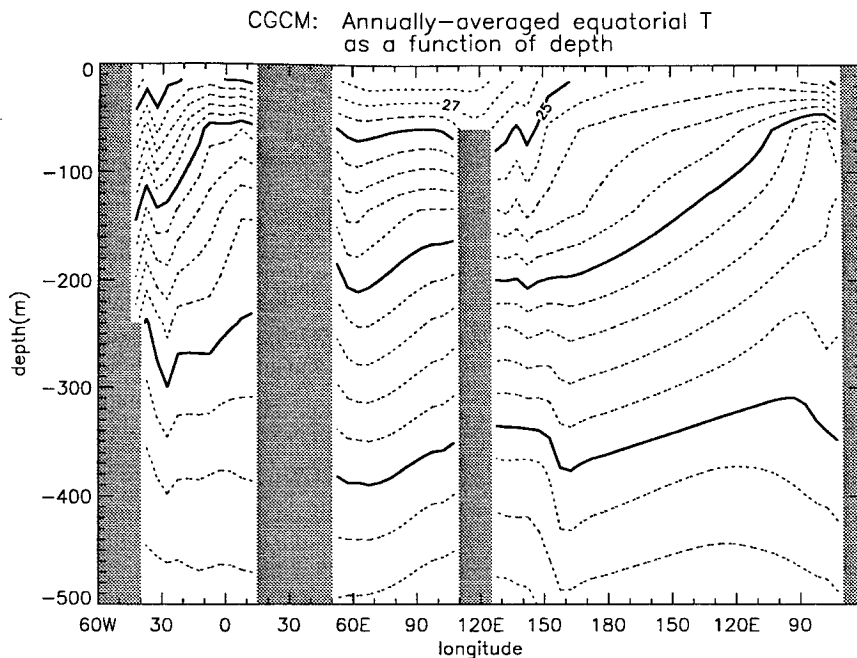


FIG. 7. Annually averaged ocean temperature ($^{\circ}\text{C}$) along the equatorial plane in the upper 500 m.

lacking within the model, uniformly cold water can rise to the surface across the entire Pacific basin, preventing the formation of a model warm pool.

3. Interannual variability

Interannual variability of equatorial SST during the first 30 years of the simulation is shown in Fig. 9. Since SST is not computed by the model precisely on the equator but at 2°S and 2°N , we define the equatorial value as the average based upon these two locations. The anomalies are defined with respect to the annual cycle. In addition, a small trend that is negligible after the first decade of the simulation has been removed.

Anomalies propagating westward across the entire width of the Pacific basin can be seen in Fig. 9, along with eastward propagating anomalies in the Indian Ocean that are more prominent during the latter half of the period. These eastward propagating anomalies will be discussed in the next section. The magnitude of the anomalies is of order 0.5°C , which is weak in comparison to the few degrees characteristic of observed ENSO anomalies. However, this magnitude is observed only within a degree or two of latitude from the equator. In the low-resolution model, anomalous heat flowing into a grid box is spread out over a relatively large volume, diminishing its ability to change the grid-box temperature. The 0.5°C warming in the CGCM anomalies represents an average across two grid boxes of total width 8° lat, while the observed anomalies decay to zero from their maximum values well within this

distance. This suggests that the observed and model anomalies of heat content within the surface layer are closer than appears from a comparison of the anomaly amplitudes.

Westward propagating anomalies can be seen in other fields, such as zonal-wind stress, rainfall, and the surface energy flux: atmospheric and oceanic variability along the equator are coupled in this particular anomaly. We have attempted to isolate this mode of variability using EOF analysis. The gravest EOF of equatorial SST (i.e., the mode representing the largest amount of variance) is shown in Fig. 10a, along with its principal component and the corresponding spectrum. This EOF has its largest amplitude in the Pacific and increases in the direction of the Indian Ocean. The principal component is characterized by an interannual timescale, with the largest spectral estimate corresponding to a period near 20 months.

Since EOFs partition variability using functions that are separable with respect to space and time, propagating features are represented by a pair of EOFs in quadrature (see below). The second EOF of equatorial SST represents nearly the same amount of variance and has a similar spatial structure and principal component, as shown in Fig. 10b. As a test of whether the first two EOFs represent a propagating mode, we can estimate the period from the phase lag between the two principal components and see whether this is consistent with the spectral peak near 20 months. The correlation between the first two principal components (not shown) has a maximum of 0.6 when the second component leads the

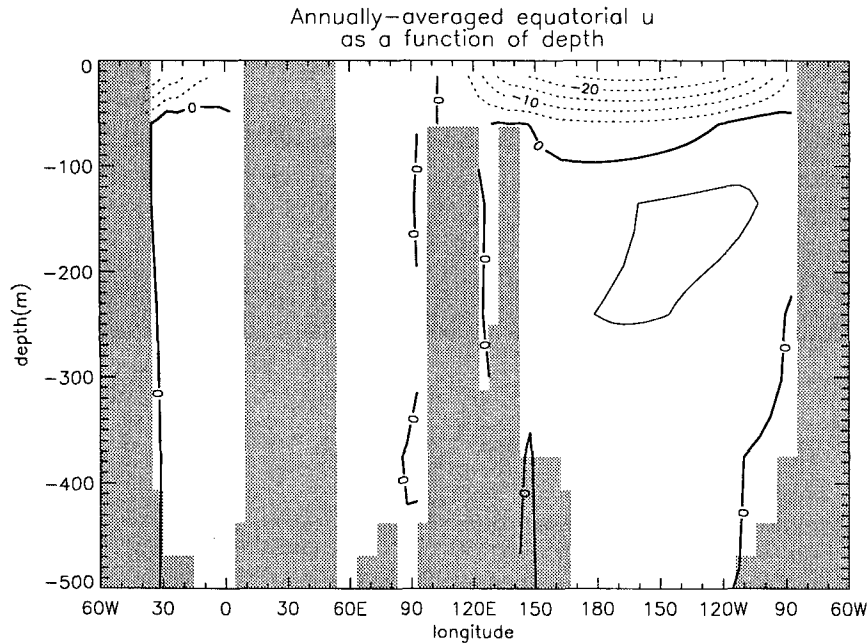


FIG. 8. Annually averaged zonal current (cm s^{-1}) along the equatorial plane in the upper 500 m.

first between 4 and 6 months. If we heuristically represent the propagating feature as $\cos(kx - \omega t)$, equal to $\cos kx \cos \omega t + \sin kx \sin \omega t$, then the first principal component can be identified with $\cos \omega t$ and the second

with $\sin \omega t = \cos[\omega t + (\pi/2)] = \cos \omega(t - t_0)$. Taking t_0 equal to -5 months, ω can be estimated as $-(\pi/2t_0)$, which corresponds to a period of 20 months, consistent with the spectra in Fig. 10. (Given that the prop-

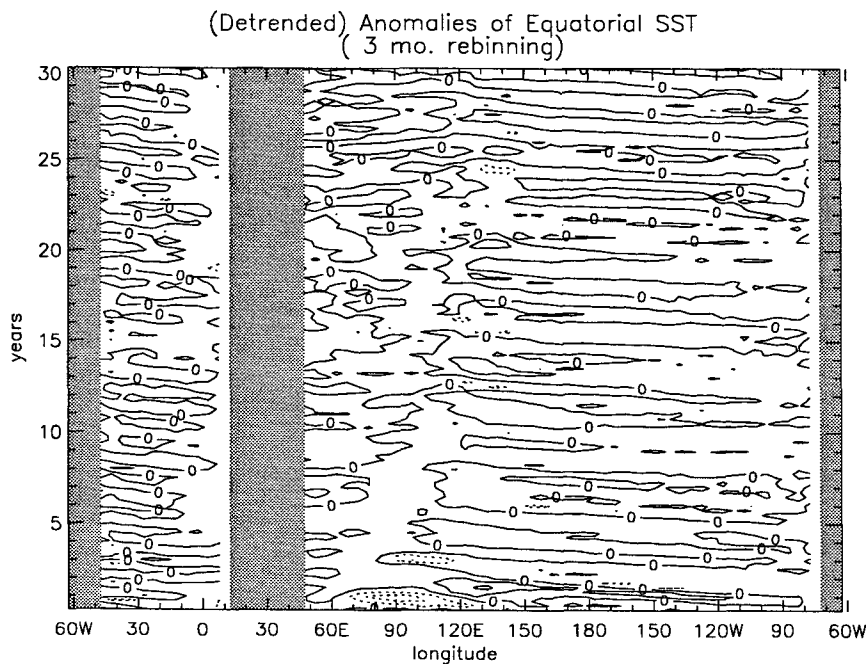


FIG. 9. Anomalies of equatorial SST defined as departures from the annual cycle. The contour interval is 0.5°C . The shaded areas near 30°E and 60°W correspond to Africa and South America, respectively. A 3-month running mean has been used to smooth the anomalies.

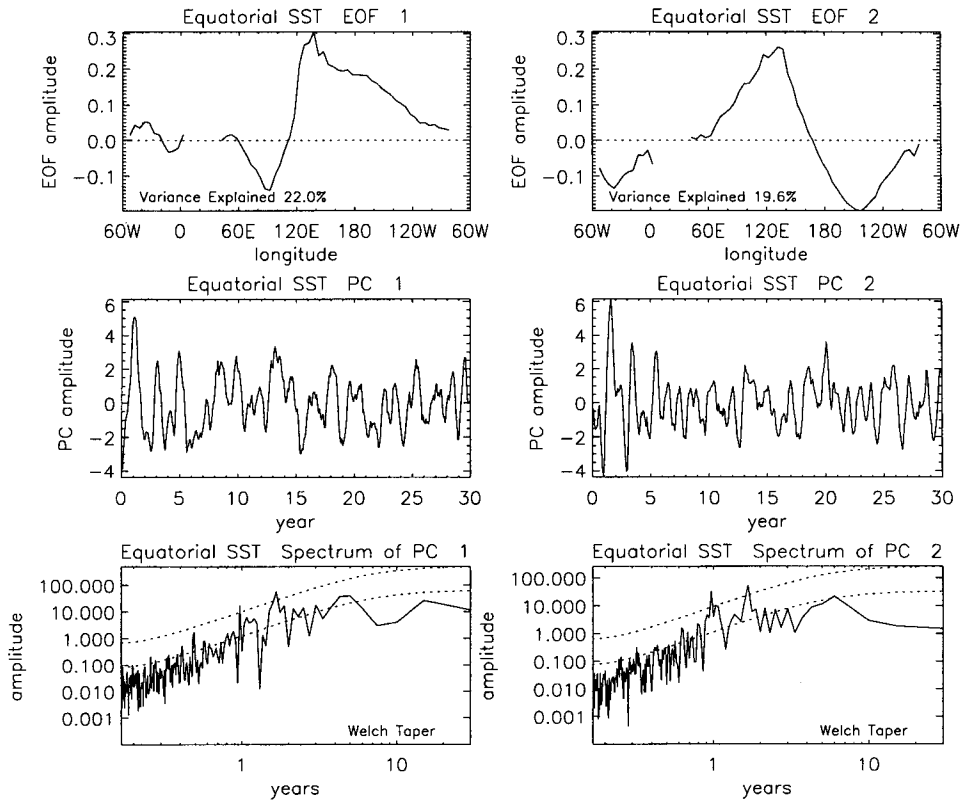


FIG. 10. The (a) first and (b) second EOFs of equatorial SST (detrended) anomalies, along with principal components and their corresponding spectra. The lower dashed line in the spectrum is the red-noise spectrum considered as a null hypothesis. Estimates of a red spectrum will lie below the upper dashed line at all periods 95% of the time.

agating features in Fig. 10 are only approximately sinusoidal, this agreement is probably better than it deserves to be.)

EOF analysis was repeated with equatorial anomalies of wind stress, rainfall, evaporation, and total surface heating. The EOFs and principal components in each case were dominated by a leading pair that resembled the gravest pair derived from the SST anomalies shown in Fig. 10. This pair also emerged in SVD analysis (cf. Bretherton et al. 1992) of SST and wind stress, along with SST and rainfall, for example, and appears not to depend upon any particular method of analysis.

By correlating the EOFs of SST, wind stress, and rainfall, spatial relations between these fields can be derived. Rainfall was found to peak roughly 10° of longitude to the west of the SST anomaly and zonal wind stress peaked 30° of longitude to the west. The coincidence of the SST and rainfall anomalies and the westward displacement of surface zonal wind anomalies is consistent with observations (e.g., Rasmusson and Carpenter 1982), and both the propagating and stationary modes of variability found in

models (e.g., Zebiak 1986; Philander et al. 1992; Lau et al. 1992).

The propagating features shown in Fig. 10 resemble the “ENSO-like” variability found in the low-resolution models of Meehl (1990) and Lau et al. (1992). Westward propagation is also exhibited by the composite anomalies of Rasmusson and Carpenter (1982), constructed using observations of six ENSO events, which originate near the South American coast before moving west toward the date line. What makes the present model variability merely ENSO-like and distinguishes it from more accurate simulations of ENSO variability is the inability of a low-resolution OGCM to capture certain physical processes such as variations in the thermocline depth that are fundamental to the observed variability (e.g., Wyrtki 1975). This brings us to the mechanisms underlying the model variability.

To diagnose the physical processes fundamental to the westward propagating mode, we have calculated the contributions to the SST anomaly, using the heat budget of the first OCGM layer. The anomaly evolves according to

$$\begin{aligned} \partial_t T' = & -\bar{u} \partial_x T' - u' \partial_x \bar{T} - u' \partial_x T' - \bar{v} \partial_y T' \\ & - v' \partial_y \bar{T} - v' \partial_y T' - \bar{w} \partial_z T' \\ & - w' \partial_z \bar{T} - w' \partial_z T' + \frac{Q'}{(C_p \rho \Delta z)}, \quad (1) \end{aligned}$$

where “primes” denote anomalous quantities; “bars” denote mean values (consisting of the annual cycle plus the small trend); the zonal, meridional, and vertical currents are represented by u , v , and w ; and Q represents the surface flux of heat into the ocean. (Here, C_p is the specific heat of seawater, ρ its density, and Δz represents the depth of the first ocean layer.)

Variability on all timescales contributes to the tendency of SST given by (1). We would like to isolate the tendency of SST corresponding solely to the westward propagating mode. Our approach is to multiply (1) by the first principal component of equatorial SST (cf. Fig. 10), corresponding to the westward propagating mode, and sum over the length of the simulation. (We repeated the analysis using the second mode of the pair corresponding to westward propagation and found no significant differences.) This sum, or inner product, is normalized so that it equals the standard deviation of the westward propagating component of each term in the equation. This is described more completely in the appendix. Our inner product is identical to the regression coefficient used by Lau et al. (1992), except for a multiplicative constant. Use of the inner product is analogous to applying a Fourier transform to Eq. (1) in order to isolate variability at a particular frequency. In fact, to the extent that the principal component corresponding to the westward propagating mode is sinusoidal, this is exactly what we have done.

Variability at other timescales is removed from (1) as a result of the orthogonality of the principal components, with two exceptions. Either through the nonlinear terms, or through the annual cycle that is included in the mean quantities of (1), variability at other timescales can drive the westward propagating mode. Both of these effects were found to be small. Along the equator, the model’s annual cycle is largest in the East Pacific, where the propagating mode is relatively small.

Before considering the physical processes leading to westward propagation via (1), we briefly discuss two mechanisms for coupled ocean–atmosphere variability in the context of this equation: namely, the “Bjerknes” mechanism where surface warming results from a diminished upwelling velocity, and the “Wyrтки” mechanism where surface warming results from the upwelling of anomalously warm subsurface water. Bjerknes (1969) noted the relation between easterly wind stress and equatorial upwelling. He argued that the strength of the easterlies depends in part upon the zonal temperature gradient between the cold tongue and the warm pool. He hypothesized that a slackening of the easterlies would reduce the upwelling, causing warming of the cold tongue, a reduction of the zonal tem-

perature gradient, and a further weakening of the easterlies. That is, Bjerknes argued that the term $w' \partial_z \bar{T}$, where w' is controlled by the strength of the anomalous easterlies (which in turn is determined by the zonal distribution of T'), gives rise to an instability coupling the equatorial ocean and atmosphere. (Because of continuity, the term $v' \partial_y \bar{T}$ also contributes to warming, according to Bjerknes’ hypothesis.)

Based upon observations of equatorial SST, winds, and sea level, Wyrтки (1975) proposed another mechanism, whereby a relaxation of the trades excites an eastward propagating oceanic Kelvin wave. This wave acts to deepen the thermocline so that upwelling water now originates above this level where temperatures are relatively warm. Battisti (1988) demonstrated that this is the process leading to warming of the East Pacific SST in the Cane–Zebiak model. In this latter model, the dominant contribution to the budget of anomalous SST is the term $\bar{w} \partial_z T'$, approximated as $\bar{w} [(T' - T'_{\text{sub}})/H]$, where T'_{sub} represents the temperature of the water upwelling into the surface layer, and H is the depth over which this water travels. As such, $\bar{w} \partial_z T'$ is the sum of two terms: $\bar{w} T'/H$, which acts as damping, and $\bar{w} T'_{\text{sub}}/H$. In the Cane–Zebiak model, T'_{sub} is parameterized in terms of the thermocline displacement: a deepening thermocline causes the upwelling water to originate at an anomalously warm isotherm, leading to warming of the surface as suggested by Wyrтки. This process is most prominent in the East Pacific, where the mean upwelling is large and the thermocline is shallow so that T'_{sub} is sensitive to its displacement.

In Fig. 11, we show the inner product of various terms in (1) with respect to the gravest principal component of equatorial SST.¹ The product is computed with the terms leading or lagging the principal component by up to a year in order to show the evolution of the mode, as well as how the relative importance of various physical processes changes as the mode moves west. The inner products with respect to the nonlinear terms have been omitted, since these are small in comparison. Positive values mean the term acts to warm the surface waters. Figure 12 shows the inner product of the same principal component with respect to anomalies of SST, zonal wind stress, rainfall, evaporation, zonal and meridional currents, upwelling, and the temperature of the second ocean model layer beneath the surface. These products are useful in interpreting the individual terms of the SST budget. As before, the product has been normalized so that it equals the standard deviation of the anomaly component corresponding to westward propagation. All of these quantities are eval-

¹ The tendency of ocean temperature in the OGCM is computed using the flux form of (1) rather than the advective form [i.e., the finite-difference approximation of $\partial_x(uT)$ rather than $u\partial_x T$, for example]. In evaluating the advective terms in (1), we used finite-difference approximations that can be derived from the flux form used by the OGCM.

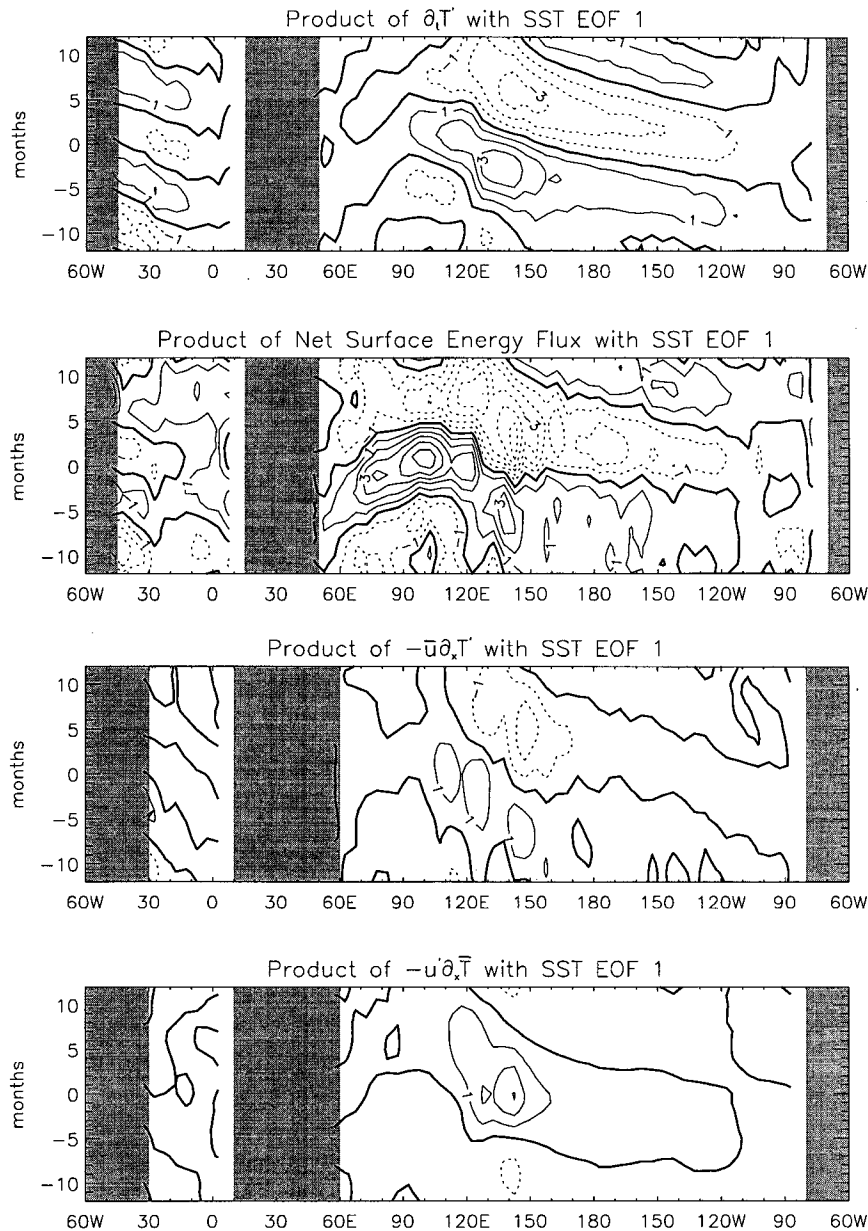


FIG. 11. Inner product of the first principal component of equatorial SST, corresponding to the westward propagating mode, with respect to various terms in the SST tendency equation ($\times 10^{-8} \text{ } ^\circ\text{C s}^{-1}$). The net surface energy flux has been divided by $\rho C_p \Delta z$.

uated at the equator, except for the meridional current, which is evaluated at 4°N (v' at the equator is small since the anomaly is nearly symmetric about this latitude).

Figure 12a shows the inner product with respect to SST. (At zero lag, the inner product as a function of longitude is simply the gravest EOF multiplied by a constant, by definition.) The westward propagation can be divided into two stages. During the first, the anomaly originates in the Eastern Pacific and then

equilibrates, while traveling westward along the cold tongue. Rainfall anomalies (Fig. 12c) are positive but small during this stage, perhaps a reflection of the cold climatological SSTs (Fig. 2). At the western edge of the cold tongue, where the mean zonal wind passes through zero (cf. Fig. 4a), the anomaly slows and further amplifies. The climatological SST increases as the anomaly emerges from the cold tongue, and anomalous rainfall increases sharply. This reamplification is the second stage. Why the anomaly

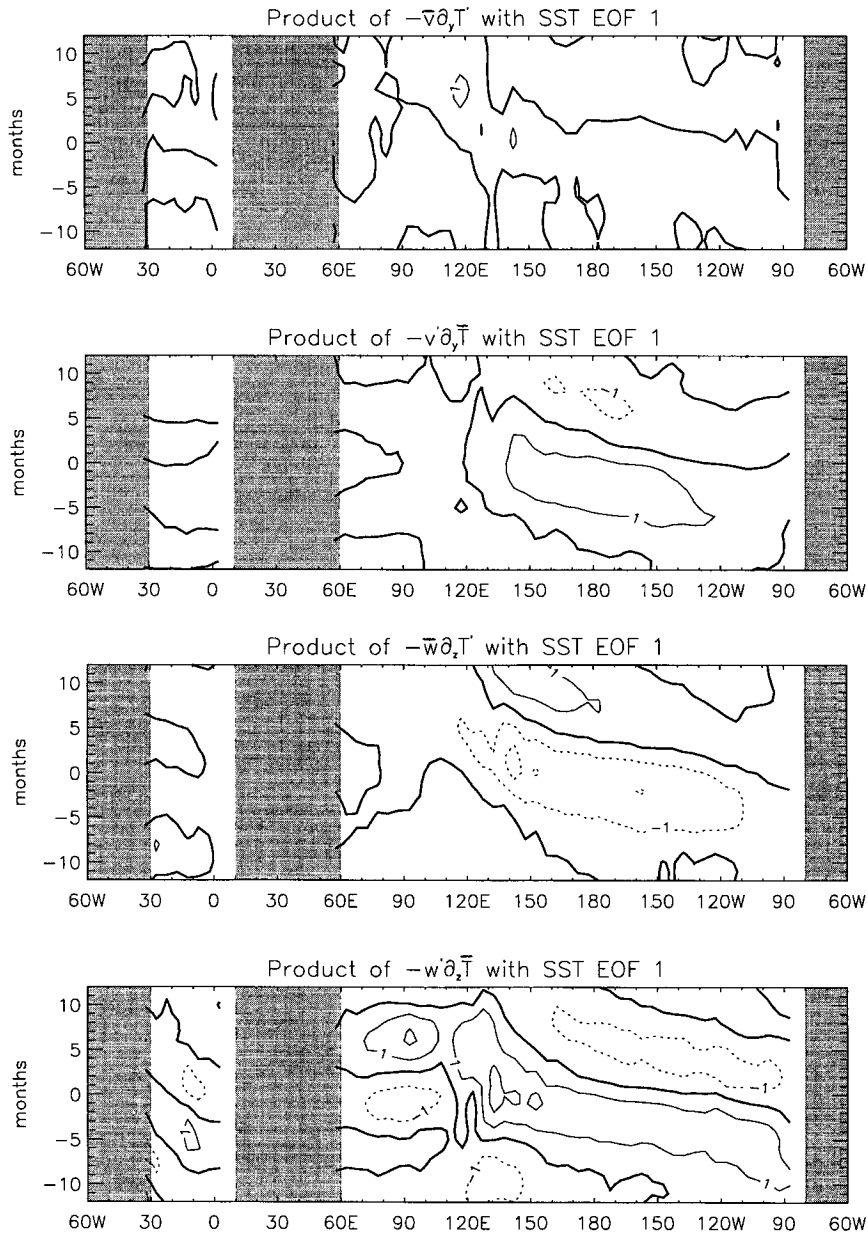


FIG. 11. (Continued)

slows and eventually dissipates will be discussed in the next section.

Within the cold tongue, Fig. 11 shows that the dominant terms are $v'\partial_y\bar{T}$, $w'\partial_z\bar{T}$, $\bar{w}\partial_zT'$, and the surface heating. The terms $v'\partial_y\bar{T}$ (Fig. 11f) and $w'\partial_z\bar{T}$ (Fig. 11h) amplify the warm anomaly. This is the signature of the Bjerknes mechanism. The zonal wind stress anomaly is westerly in this region (Fig. 12b), diminishing the total easterlies and reducing w' (Fig. 12g), the upwelling of cold water. Anomalous equatorward flow v' (Fig. 12f) contributes to the warming by advecting climatologically

warmer water into the cold tongue. Because the zonal wind stress anomaly is centered to the west of the SST anomaly, the anomalous upwelling circulation is also displaced relative to the SST anomaly and causes warming to the west, inducing westward propagation.

Warming due to the weakened upwelling circulation is balanced by the cooling due to the term $\bar{w}\partial_zT'$ (Fig. 11g). Warming beneath the surface layer is smaller and lags behind temperature changes at the surface (Fig. 12h): a signature of the predominance of model diffusion over equatorial wave dynamics, which the

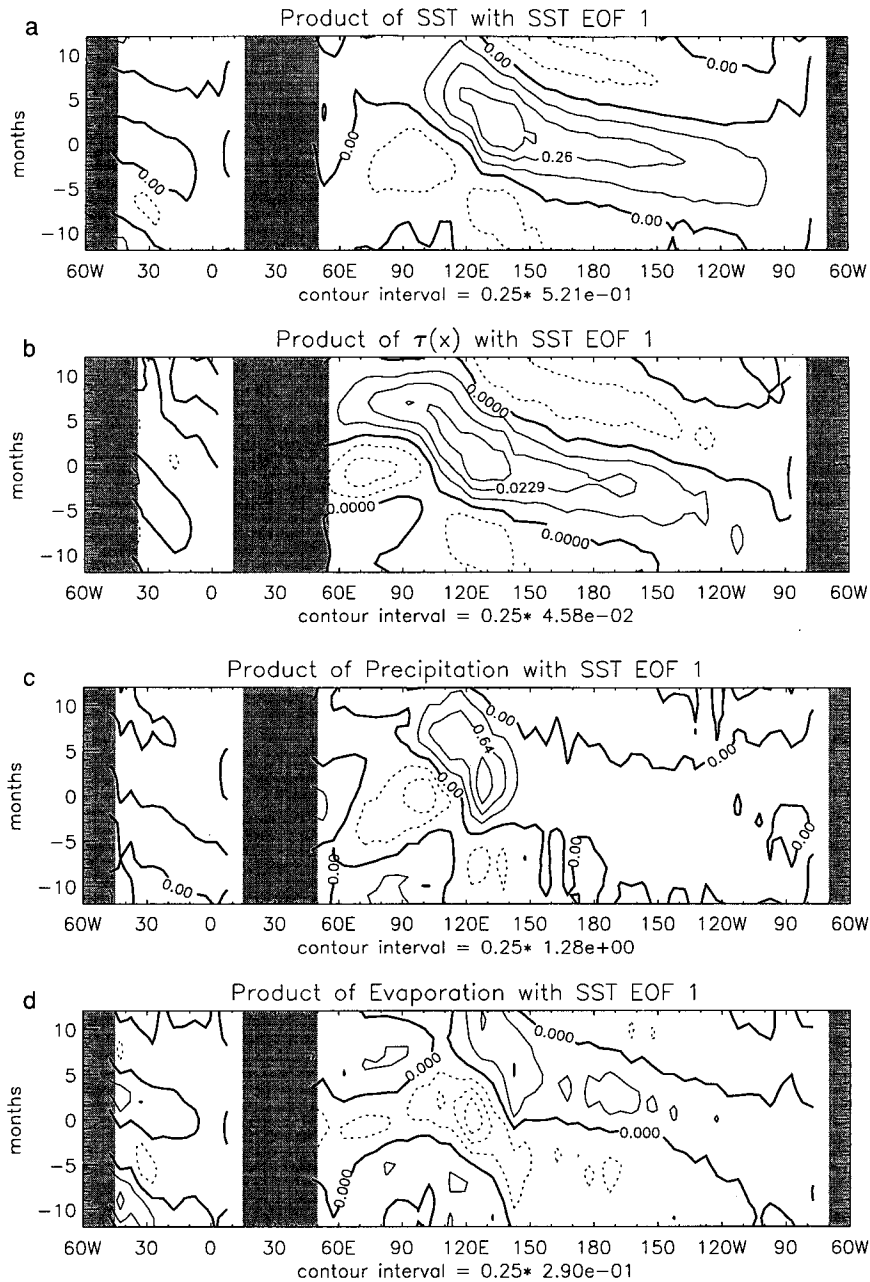


FIG. 12. Inner product of the first principal component of equatorial SST, corresponding to the westward propagating mode, with respect to anomalies of (a) SST ($^{\circ}\text{C}$), (b) zonal wind stress (dynes cm^{-2}), (c) rainfall (mm day^{-1}), (d) evaporation (mm day^{-1}), (e) zonal surface current (cm s^{-1}), (f) meridional surface current (cm s^{-1}), (g) upwelling into the surface layer (cm s^{-1}), and (h) ocean temperature in the second layer from the top ($^{\circ}\text{C}$).

model lacks the resolution to properly resolve. As a consequence, the anomaly diminishes with depth and the mean upwelling of the anomalous vertical temperature gradient opposes the warming at the surface. In this case, the behavior of the CGCM anomaly contrasts with that of the Cane–Zebiak model. In the latter, warming of T'_{sub} is greater than at the surface so that

$\bar{w}\partial_z T'$ amplifies the SST anomaly (e.g., Battisti 1988; Battisti and Hirst 1989). This difference results from the diffuse thermocline in the CGCM. Even if the subsurface isotherms are displaced by equatorial waves, the mean vertical temperature gradient is so small that T'_{sub} is hardly affected. Lau et al. (1992) have noted similar behavior in their coupled model. Their OGCM

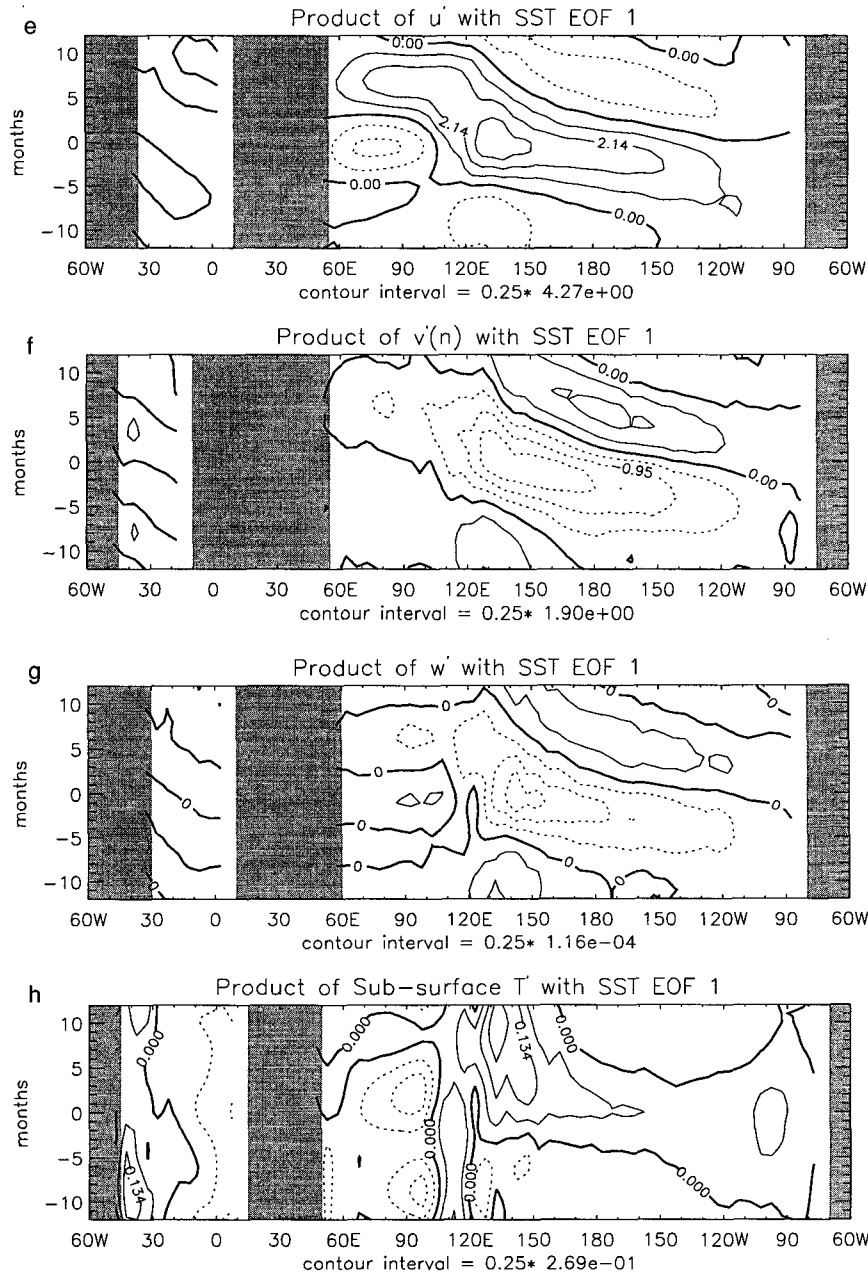


FIG. 12. (Continued)

also has a weak thermocline, which they attribute to the large diffusion associated with low resolution. Consequently, mean upwelling of the anomalous temperature gradient does not amplify the anomaly. Neelin (1991) has shown that in the presence of a sharp thermocline this process not only reinforces surface warming, but also favors eastward propagation, in opposition to the westward propagation induced by the anomalous upwelling. This suggests that westward propagating

anomalies should be a generic property of models that are unable to simulate a realistically sharp thermocline—for example, models with a low-resolution OGCM as described here and by Meehl (1990) and Lau et al. (1992).

The term $\bar{u}\partial_x T'$ (Fig. 11c) represents the Doppler effect. This term merely advects the anomaly with the mean zonal current, and does not contribute to growth. As the anomaly approaches the western edge of the

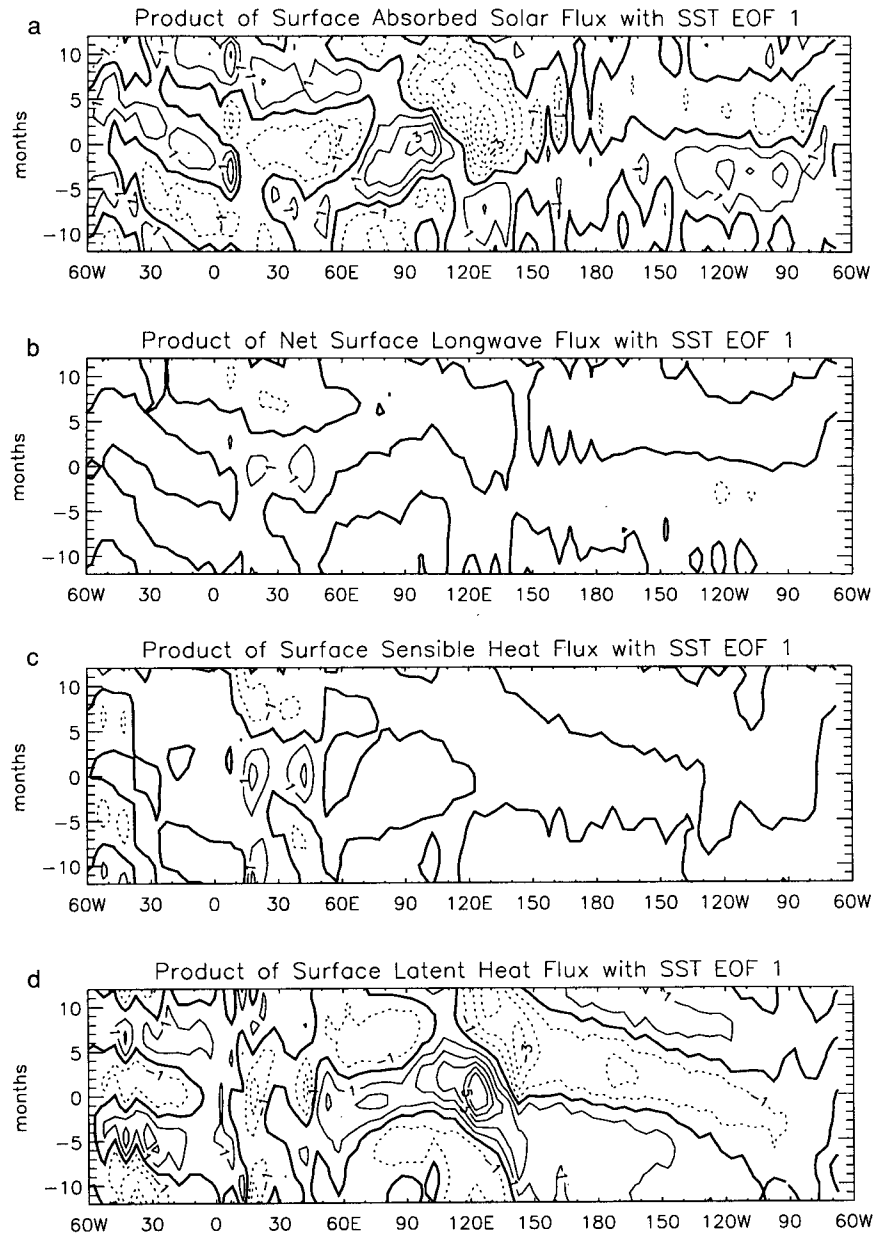


FIG. 13. Inner product of the first principal component of equatorial SST, corresponding to the westward propagating mode, with respect to contributions to the surface energy flux anomaly, divided by $\rho C_p \Delta z$ ($\times 10^{-8} \text{ } ^\circ\text{C s}^{-1}$): (a) surface solar radiation, (b) surface longwave radiation, (c) latent heating, and (d) sensible heating.

cold tongue, the term $u' \partial_x \bar{T}$ (Fig. 11d) contributes to warming since the zonal gradient of mean SST is large in this region (cf. Fig. 2). Since u' is largely coincident with the anomalous zonal wind stress, this term should favor westward propagation. Despite the increasing importance of this term, the rate of westward propagation decreases. The mechanism responsible for the dissipation of the anomaly will be discussed in the next section.

4. The role of surface heating

The surface energy flux $Q'/\rho C_p \Delta z$ is shown in Fig. 11b to be comparable to the advective terms. The inner product of the individual components of the surface flux—solar and longwave radiation, along with the latent and sensible heating—are shown in Fig. 13. The surface flux anomaly largely reflects variations in solar (Fig. 13a) and latent heating (Fig. 13c). Sensible heat-

ing (Fig. 13d) generally has the same sign as the latter but is of smaller amplitude—consistent with the small observed tropical Bowen ratio (e.g., Sarachik 1974). Solar heating is correlated with anomalous rainfall (Fig. 12c), since deep convection acts to shield the surface from solar radiation in the model. Longwave anomalies (Fig. 13b) oppose the solar flux but are of much smaller magnitude. Apparently, SST increases are accompanied by a rise in boundary layer humidity, so that increased longwave fluxes away from the surface are nearly compensated by increased downward fluxes from boundary layer water vapor, leaving the net longwave flux at the surface practically unchanged.

The surface energy flux is better correlated with respect to the tendency of SST, rather than SST itself, as shown by a comparison of Fig. 11b to Fig. 11a and 12a. Surface fluxes do not begin to remove heat from the ocean until the SST anomaly is near its peak. Weare (1983) suggested that there is a similar phase lag between the observed surface heating and ENSO SST anomalies, so that surface fluxes initially reinforce the warm anomaly. While the surface flux is typically parameterized as Newtonian cooling, the CGCM behavior along with Weare’s analysis suggest that its role is more complicated.

The latent heat flux (Fig. 12d) and surface heating (Fig. 11b) anomalies are displaced westward of the SST anomaly in Fig. 12a, almost coincident with the zonal wind stress anomaly (Fig. 12b). Wind anomalies can affect latent heating rates, according to bulk parameterizations of evaporation. (Although bulk parameterizations of surface fluxes probably oversimplify the behavior of the AGCM’s boundary layer parameterization, we assume that bulk formulas are accurate enough to be of interpretive value.) Here,

$$LE = L\rho_{air}C_D|u|(q_{surf} - q_{air})$$

$$= L\rho_{air}C_D|u|[q^*(T) - rq^*(T_a)]$$

$$LE' = L\rho_{air}C_D|u|(1 - r)\partial_T\bar{q}^*T' + L\rho_{air}C_D$$

$$\times [q^*(\bar{T}) - rq^*(\bar{T}_a)](|\bar{u} + u'| - |\bar{u}|), \quad (2)$$

where $q^*(T)$ is the saturation specific humidity as a function of the sea surface temperature T , r is the relative humidity, and T_a is the air temperature. The relative humidity and the air–sea temperature difference ($T - T_a$) have been assumed constant for the purposes of discussion.

The first term of (2) is the basis for the Newtonian cooling parameterization of the surface energy flux. The effects of anomalous radiative heating can be parameterized in a similar manner since surface solar anomalies are approximately coincident with cloud cover anomalies, which in turn are related to SST anomalies. (Note the correspondence between the surface solar, rainfall, and SST anomalies in Figs. 13a, 12c, and 12a, respectively.)

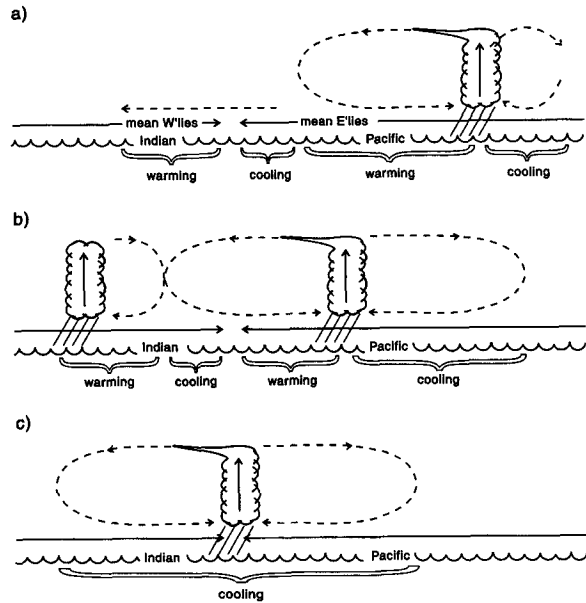


FIG. 14. Schematic of the effect of evaporation in forcing SST. (a) In a region of mean easterlies, such as the equatorial Pacific, the anomalous convective circulation over a warm SST anomaly reduces the total wind—and thus evaporative cooling of the ocean surface—to the west of the SST anomaly, causing propagation in this direction. As the anomaly approaches the Indian Ocean (a region of mean westerlies), anomalous easterlies are triggered in this region, reducing evaporation and warming the ocean. (b) In response to the warming, an anomalous convective circulation forms on the western edge of the easterlies, propagating to the east as a result of wind–evaporative feedbacks. (c) The Pacific and Indian Ocean convective anomalies merge and dissipate, partly as a result of evaporative cooling, where the mean zonal wind passes through zero.

The second term relates changes in the latent heat flux to wind anomalies. Consider an anomalous convective circulation over a warm SST anomaly as depicted in Fig. 14a. In a region of mean easterlies, such as the Pacific basin, the total wind and the rate of evaporative cooling are reduced by anomalous surface westerlies, while increased by anomalous easterlies. Thus, the anomalous convective circulation reduces the latent heat flux and causes warming to the west of the SST anomaly, inducing propagation in this direction. Consequently, in the presence of mean easterlies, anomalous westerlies cause westward propagation of SST anomalies through two mechanisms (in addition to advection by the zonal mean current): reduced upwelling in the cold tongue and the wind–evaporative feedback.

In a region of mean westerlies, such as the equatorial Indian Ocean, the direction of propagation resulting from the wind–evaporative feedback is reversed, as the total wind and rate of evaporative cooling are diminished to the east of a convective anomaly. Eastward propagation is displayed in the model Indian Ocean, as depicted in the SST anomalies of Fig. 9. The inner product maps of several quantities such as the SST ten-

dency, surface energy flux, zonal wind stress, evaporation, and precipitation suggest that this propagation is related to the approach of the Pacific coupled mode.

For example, eastward propagating anomalies can be seen in the SST tendency (Fig. 11a), first appearing in the eastern Indian Ocean near -5 months as the Pacific anomalies begin to amplify rapidly near the western extent of the cold tongue. The largest contribution to the SST tendency within the Indian Ocean arises from the surface energy flux (Fig. 11b). Warming of SST is predominately a result of a reduced surface latent heat flux (Fig. 13c) associated with anomalous surface easterlies (Fig. 12b), along with increased solar heating (Fig. 13a) related to reductions in cloud cover (as inferred from the precipitation anomaly in Fig. 12c). Why the easterlies increase over the Indian Ocean as the Pacific anomaly approaches is unclear. One possibility is that the Hadley circulation, including the zonally averaged surface easterlies, increases in strength as the Pacific anomaly amplifies near the western edge of the cold tongue. In any case, the effect of increased easterlies is to reduce the total wind and evaporative cooling.

In response to surface heating, a weak convective anomaly forms at the western edge of the easterlies (Fig. 12c). Wind–evaporative feedbacks favor eastward propagation of this anomaly along with its eventual merger with the Pacific anomaly. This propagation and merger is displayed by the SST tendency in Fig. 11a, although it is less obvious in SST itself (Fig. 12a). Because the Indian Ocean anomaly is weak in comparison to the Pacific anomaly, eastward propagation is possibly obscured by other modes of variability in the SST field. Weak amplitudes perhaps result from the competing effects of the easterlies, whereby warming due to wind–evaporative feedbacks is partially offset by anomalous upwelling. Consequently, amplification of the Indian Ocean convective anomaly proceeds slowly in comparison to the Pacific mode.

The Pacific anomaly slows markedly upon approaching the longitude where the mean zonal wind passes through zero (near 100°E in Fig. 4). The region of warming by wind–evaporative feedbacks cannot extend past the zero-wind line, since westerly surface flow to the west of this longitude reinforces rather than opposes the mean winds. Eastward propagation of the Indian Ocean anomaly is similarly bounded by the zero-wind line. Figure 13d shows that by $+5$ months, when both the Pacific and Indian anomalies have arrived at this longitude, the anomalous latent heat flux cools the ocean across the entire extent of the SST anomaly, since the anomalous winds everywhere reinforce the mean (Fig. 12b). The westward approach of the Pacific anomaly and excitation of the Indian Ocean mode, along with the merger and decay of both anomalies at the zero-wind line is summarized in Figs. 14a–c.

The behavior of the equatorial anomalies in the CGCM suggests that surface fluxes—particularly the evaporative component—do more than simply damp SST anomalies. Wind–evaporative feedbacks are suggested to be the cause of the spatial offset of the surface energy flux and SST anomalies, so that evaporation leads to amplification and propagation of the Pacific mode. Evaporative feedbacks allow SST anomalies to affect the climate over a much broader area by forcing a large-scale circulation that affects the wind stress and evaporative rates far from the original anomaly. For example, the eastward traveling anomalies in the Indian Ocean appear to originate in response to the approach of a Pacific anomaly. The effects of wind–evaporative feedbacks are especially apparent in regions like the Indian Ocean where horizontal gradients of SST are small so that anomalous currents have comparatively little effect upon SST.

The relation between Indian Ocean variability and ENSO events has long been recognized. Villwock and Latif (1995, manuscript submitted to *J. Phys. Oceanogr.*) show that the gravest EOF of Indian Ocean SST corresponds to basinwide warming in response to ENSO. Other studies (e.g., Meehl 1987, 1993) have also noted a correlation between weak Indian monsoons and ENSO. To what extent wind–evaporative feedbacks contribute to the observed covariability of Pacific and Indian Ocean SST is unclear. The present CGCM presumably overestimates the effect of this mechanism by allowing the model Pacific anomalies to propagate as far west as the Indonesian Archipelago, whereas the observed warming diminishes west of the date line. Nonetheless, observed Pacific SST anomalies appear to modulate the winds over the Indian Ocean, as shown by Latif and Barnett (1995), who forced an empirical wind stress model with that part of the ENSO SST anomaly confined to the Pacific. It remains unknown whether these wind anomalies change the evaporation sufficiently to account for the SST variability observed in the Indian Ocean. Meehl (1993) noted that wind–evaporative feedbacks would be amplified by changes in the ocean mixed-layer depth. Diminished winds, which reduce evaporation, decrease the depth of the ocean mixed layer through a reduction in turbulent mixing, so that surface heating is concentrated over a shallower layer.

Villwock and Latif (1995, manuscript submitted to *J. Phys. Oceanogr.*) suggest an alternative mechanism by which the Indian Ocean warms in response to Pacific SST anomalies. Reduced convective cloud cover in the east Indian Ocean associated with anomalous low-level divergence increases solar heating of the ocean surface. This mechanism contributes to warming of the Indian Ocean in our model as well, as shown by the maps of precipitation and surface solar heating (Fig. 12c and Fig. 13a), although the warming is more apparent in SST tendency (Fig. 11a) as opposed to SST itself (Fig. 12a).

5. Conclusions

We have described how atmospheric and oceanic variability interact in a low-resolution coupled GCM to produce tropical anomalies with interannual timescales. In this context, "low" resolution means that the equatorial ocean waveguide and thermocline are not well resolved by the model, even though the $4^\circ \text{ lat} \times 5^\circ \text{ long}$ resolution is sufficient to resolve most features of the atmospheric circulation.

Neelin et al. (1992) noted that tropical interannual variability does not necessarily arise from the coupling of atmospheric and oceanic GCMs. The model surface winds may be insufficiently sensitive to SST, for example, or the model may drift into a new and unrealistic equilibrium, even if the atmospheric and oceanic components are well behaved when integrated separately. Coupled simulations are a more stringent test of the individual models. Nonetheless, we have found tropical coupled modes in our simulation of 110 years of unforced variability. We have identified certain features of these modes that we believe are characteristic of the modes found in all low-resolution models exhibiting coupled variability. First, the amplitude of the Pacific SST anomalies are relatively small (of order 0.5°C in our model) in comparison to observed ENSO anomalies as well as the magnitude of variability found in higher resolution CGCMs (e.g., Philander et al. 1992). The anomaly in our low-resolution model represents an average across a meridional width of at least two grid boxes or 8° of latitude. Observed SST anomalies decay to zero from their maximum equatorial values well within this distance and we estimate that the total surface heat content may be closer to observed values if the broader meridional extent of low-resolution model anomalies are taken into account. The larger dissipation present in a low-resolution model may also limit the magnitude of the anomalies.

The model Pacific anomalies propagate to the west, similar to the variability found in the low-resolution simulations of Meehl (1990) and Lau et al. (1992). Westward propagation in the CGCM resembles the composite ENSO anomaly constructed by Rasmusson and Carpenter (1982), which originates near the South American coast before propagating toward the date line. In the present model, anomalies propagate unrealistically far to the west, arriving at the Indonesian archipelago before decaying. We have identified three processes which, in the presence of mean easterly winds, lead to westward propagation. First, there is downwind advection by the mean zonal current. Second, there is the Bjerknes mechanism whereby anomalous westerlies (which peak to the west of the SST anomaly) reduce the rate of upwelling of cold subsurface water. And third, there is the wind- evaporative feedback.

Observed ENSO anomalies along with those from high-resolution simulations are largely confined to the

East and Central Pacific, whereas the anomalies described in this study and those of Meehl (1990) and Lau et al. (1992) continue into the West Pacific. Meehl (1990) argues that anomaly propagation into the West Pacific in his low-resolution CGCM results from the model's inability to simulate the West Pacific climate, and, in particular, the Warm Pool. He suggests that the anomaly behavior within the East Pacific is nonetheless modeled correctly. However, we believe that within the East Pacific, not all physical processes fundamental to the anomaly are well simulated in low-resolution models and that westward propagation is exaggerated as a result. In the analytic model of Neelin (1991), westward propagation due to the effects described above is opposed by the upwelling of anomalously warm subsurface water—that is, the Wyrtki mechanism—a process which is shown by Neelin to favor eastward propagation. The balance of these two effects leads to localized solutions. [Wakata and Sarachik (1991) have shown that restriction of anomalies to east of the date line in the Cane-Zebiak model can also come about since properties of the mean state that favor warming such as a large upwelling rate and a shallow, intense thermocline are restricted to this region.] In the coupled model considered here, ocean temperature anomalies decay beneath the surface layer so that the advection of the anomalous temperature gradient by mean upwelling acts as damping: that is, T'_{sub} is less than the anomalous SST. We have argued that this occurs because our model thermocline is unrealistically diffuse, so that displacements of the isotherms by equatorial dynamics hardly change the temperature of the upwelling water. We believe that the diffuse thermocline arises in our model as a result of the large dissipation associated with the low resolution. To the extent that all low-resolution models have comparable dissipation and underestimate the intensity of the thermocline, the Bjerknes mechanism will be favored over the Wyrtki mechanism, and westward propagation will occur.

We have emphasized the role of surface energy fluxes—in particular evaporative fluxes—in creating interannual coupled variability. Simplified models that illuminate much of the physics underlying ENSO typically treat this process as a negative feedback. Such models demonstrate that ENSO variability can arise solely from the redistribution of heat by an anomalous ocean circulation and does not require external forcing by means of surface fluxes. However, the CGCM suggests that surface fluxes, in particular through wind- evaporative feedbacks, can contribute to the growth and propagation of SST anomalies to an extent that is comparable to advective processes. It is possible that the CGCM exaggerates the importance of the surface fluxes compared to the advective terms, since certain advective processes fundamental to ENSO depend upon a sharp thermocline, which is underestimated by our model. Nonetheless, the behavior of surface fluxes in our model is consistent with the analysis of Weare

(1983), wherein observed surface fluxes reinforce the ENSO anomaly during its initial warming.

We have also shown how wind–evaporative feedbacks and anomalous surface energy fluxes link variability in our model’s Pacific and Indian Ocean basins. Latent heat flux anomalies allow SST anomalies to trigger anomalies across zero-wind lines, which the original ocean anomalies are themselves incapable of crossing. Wind–evaporative feedbacks are particularly important in ocean basins where horizontal gradients of SST are small, as in the Indian Ocean, and advective fluxes are comparatively unimportant. Meehl (1987, 1993) and Nicholls (1978) have suggested that such feedbacks in response to local convection lead to biennial variability in the circulation of the Indian Ocean. We have also cited evidence (Latif and Barnett 1995) that the Pacific SST anomalies associated with ENSO excite surface wind anomalies within the Indian Ocean, although it remains to be seen whether the corresponding anomaly in evaporation has a significant effect upon Indian Ocean SST.

Other means by which surface fluxes influence tropical coupled variability have been proposed. Villwock and Latif (1995, manuscript submitted to *J. Phys. Oceanogr.*) suggest that the reduction in cloud cover over the East Indian Ocean, associated with a shift in the Walker circulation during ENSO, increases the sunlight absorbed at the ocean surface, resulting in warming. Waliser et al. (1994) find that convective cloud cover reduces surface solar radiation and opposes ENSO warming in the central Pacific. In contrast, Tett (1995) finds in a CGCM simulation that solar heating can amplify ENSO anomalies, as marine stratocumulus cloud cover is reduced in response to warmer SSTs. And Miller and DelGenio (1994) have described how cloud cover feedbacks associated with deep convection can lead to interannual variability of tropical SST if the convective response to the warming is delayed by a few months.

We have described how wind–evaporative feedbacks can generate propagating modes of coupled variability, and it is of interest whether such feedbacks contribute significantly to the propagation of observed coupled modes, such as the composite ENSO modes of Rasmusson and Carpenter (1982). Seager (1989) simulated ENSO events between 1970 and 1987, using bulk parameterizations of surface fluxes instead of a linear restoring term. Surface flux anomalies arising from wind–evaporative feedbacks were found to be comparable to the advective terms of the SST tendency equation in the Central Pacific. Westward propagation is also observed as part of the seasonal cycle of the East Pacific (Horel 1982), as warming of the cold tongue begins during the Northern Hemisphere winter at the South American coast, before propagating westward. The coastal warming is associated with surface convergence and westerly inflow from the west. It remains to be seen whether reduced evaporation under the west-

erlies is important to displacing the warm water away from the coast, in comparison to advective processes such as upwelling.

Since the 1982–1983 ENSO, observed anomalies have tended to propagate eastward from the date line toward South America. This suggests that the relative importance of processes that favor westward propagation—such as reduced upwelling and wind–evaporative feedbacks—have become less important compared to processes favoring propagation to the east—such as upwelling of anomalously warm water associated with displacement of the thermocline. A higher-resolution model, capable of simulating a realistically sharp thermocline, will be required to model this change in ENSO behavior.

Acknowledgments. We thank two anonymous reviewers, along with Tony Del Genio, Jerry Meehl, Gary Meyers, Ed Schneider, Paul Schopf, Laurent Terray, and Susan Wijffels for their helpful comments. This work was supported by a grant to the Goddard Institute for Space Studies by the NASA Office for the Mission to Planet Earth. RLM was also supported by the National Science Foundation (Grant ATM-94-22631 of the Climate Dynamics Program) and the NASA Tropical Rainfall Measuring Mission.

APPENDIX

Interpretation of the Inner Product

In section 3, we defined an inner product of the first principal component of equatorial SST with respect to various physical quantities. The purpose was to extract the variability within these quantities corresponding to the westward propagating mode. In this appendix, we define the inner product more precisely, including the normalization coefficient. We show that the inner product has the same dimensions as the physical quantity, and can be interpreted as the standard deviation of the westward propagating mode at each location. We also show how to compare the magnitude of our product with that of Lau et al. (1992), who use a slightly different normalization.

We start by decomposing equatorial SST into its n EOFs and principal components,

$$T(x_i, t_j) = \sum_n e_n(x_i) T_n c_n(t_j),$$

where $e_n(x_i)$ is the EOF and the product $T_n c_n(t_j)$ is the principal component, examples of which are the westward propagating pair of modes shown in Fig. 10. The EOFs and the principal components are orthonormal, so that

$$\sum_{i=1}^{N_x} e_m(x_i) e_n(x_i) = \delta_{m,n}, \quad \sum_{j=1}^N c_m(t_j) c_n(t_j) = \delta_{m,n},$$

where N_x is the number of model grid boxes along the equator (equal to 72) and N is the total number of months (equal to 360).

We construct an inner product P_A between a physical quantity A and either of the principal components in Fig. 10 corresponding to the westward propagating mode [which we denote as $T_w c_w(t_j)$]:

$$P_A \equiv \frac{1}{C_0} \sum_{j=1}^N A(x_i, t_j) T_w c_w(t_j),$$

where C_0 is a normalization constant.

Lau et al. (1992) choose C_0 so that the maximum inner product of SST with the westward propagating principal component is 1°C. In contrast, we set C_0 equal to $T_w \sqrt{N}$ because, as shown below, it allows the inner product at each location to be interpreted as the standard deviation of A associated with the westward propagating mode. Evidently, this choice for C_0 also allows the inner product to have the same physical dimensions as A .

First, decompose A in terms of the functions $c_n(t_j)$:

$$A(x_i, t_j) = \sum_n A_n(x_i) c_n(t_j).$$

Then the inner product is

$$\begin{aligned} P_A &\equiv \frac{1}{C_0} \sum_{j=1}^N A(x_i, t_j) T_w c_w(t_j) \\ &= \frac{1}{C_0} \sum_{j=1}^N \left(\sum_n A_n(x_i) c_n(t_j) \right) T_w c_w(t_j) \\ &= \frac{A_w(x_i)}{\sqrt{N}}, \end{aligned}$$

where $A_w(x_i) c_w(t_j)$ is the component corresponding to westward propagation and where we have chosen C_0 equal to $T_w \sqrt{N}$. Because P_A^2 equals the contribution of the westward propagating mode to the variance at each location x_i , P_A can be interpreted as the standard deviation of this mode at each location. (Note that while the total variance at each location is the sum of the variances corresponding to each mode, the total standard deviation is less than the sum of the modal standard deviations.) In general, this interpretation of the inner product cannot be extended to nonzero lag because the principal components $T_n c_n(t_j)$ are no longer necessarily orthogonal. However, to the extent that the propagating mode principal components are sinusoidal, then orthogonality remains a valid assumption, so that the inner product reflects the standard deviation of the westward propagating component even at nonzero lag.

REFERENCES

Arakawa, A., and W. Schubert, 1974: Interaction of a cumulus cloud ensemble with the large-scale environment, Part I. *J. Atmos. Sci.*, **31**, 674–701.

Barnett, T., A. D. DelGenio, and R. Ruedy, 1992: Unforced decadal fluctuations in a coupled model of the atmosphere and ocean mixed layer. *J. Geophys. Res.*, **97**, 7341–7354.

Battisti, D. S., 1988: Dynamics and thermodynamics of a warming event in a coupled tropical atmosphere–ocean model. *J. Atmos. Sci.*, **45**, 2889–2919.

—, and A. C. Hirst, 1989: Interannual variability in a tropical atmosphere–ocean model: Influence of the basic state, ocean geometry and nonlinearity. *J. Atmos. Sci.*, **46**, 1687–1712.

Bjerknes, J., 1969: Atmospheric teleconnections from the equatorial Pacific. *Mon. Wea. Rev.*, **97**, 163–172.

Bretherton, C. S., C. Smith, and J. M. Wallace, 1992: An intercomparison of methods for finding coupled patterns in climate data. *J. Climate*, **5**, 541–560.

Bryan, K., 1969: A numerical method for the study of the circulation of the World Ocean. *J. Comput. Phys.*, **4**, 347–376.

—, and M. D. Cox, 1972: An approximate equation of state for numerical model of ocean circulation. *J. Phys. Oceanogr.*, **2**, 510–514.

—, and L. J. Lewis, 1979: A water mass model of the World Ocean. *J. Geophys. Res.*, **84**, 2503–2517.

Bryden, H. L., and E. C. Brady, 1985: Diagnostic model of the three-dimensional circulation in the upper equatorial Pacific Ocean. *J. Phys. Oceanogr.*, **15**, 1255–1273.

Cane, M. A., M. Münnich, and S. E. Zebiak, 1990: A study of self-excited oscillations of the tropical ocean–atmosphere system. Part I: Linear analysis. *J. Atmos. Sci.*, **47**, 1562–1577.

Cox, M. D., 1984: A primitive equation three-dimensional model of the ocean. GFDL Ocean Group Tech. Rep. 1, 143 pp.

DelGenio, A. D., and M.-S. Yao, 1993: Efficient cumulus parameterization for long-term climate studies: The GISS scheme. *The Representation of Cumulus Convection in Numerical Models*, Meteor. Monogr., No. 46, Amer. Meteor. Soc., 181–184.

—, —, and C. E. Wendell, 1993: GCM feedback sensitivity to interactive cloud water budget parameterization. Preprints, *Fourth Symp. on Global Change Studies*, Anaheim, CA, Amer. Meteor. Soc., 176–181.

—, —, W. Kovari, and K. K.-W. Lo, 1996: A prognostic cloud water parameterization for global climate models. *J. Climate*, **9**, 270–304.

Druyan, L. M., K. P. Shah, K.-W. K. Lo, J. A. Marengo, and G. Russell, 1995: Impacts of model improvements on GCM sensitivity to SST forcing. *Int. J. Climatol.*, **15**, 1061–1086.

Emanuel, K. A., 1987: An air–sea interaction model of intraseasonal oscillations in the tropics. *J. Atmos. Sci.*, **44**, 2324–2340.

Gill, A. E., 1980: Some simple solutions for heat-induced tropical circulation. *Quart. J. Roy. Meteor. Soc.*, **106**, 447–462.

Hansen, J., G. Russell, D. Rind, P. Stone, A. Lacis, S. Lebedeff, R. Ruedy, and L. Travis, 1983: Efficient three-dimensional global models for climate studies: Models I and II. *Mon. Wea. Rev.*, **111**, 609–662.

—, I. Fung, A. Lacis, D. Rind, S. Lebedeff, R. Ruedy, G. Russell, and P. Stone, 1988: Global climate changes as forecast by goddard institute for space studies three-dimensional model. *J. Geophys. Res.*, **93**, 9341–9364.

Horel, J. D., 1982: On the annual cycle of the tropical Pacific atmosphere and ocean. *Mon. Wea. Rev.*, **110**, 1863–1878.

Jin, F.-F., and J. D. Neelin, 1993a: Modes of interannual tropical ocean–atmosphere interaction—A unified view. Part III: Analytic results in fully coupled cases. *J. Atmos. Sci.*, **50**, 3523–3540.

—, and —, 1993b: Modes of interannual tropical ocean–atmosphere interaction—A unified view. Part I: Numerical results. *J. Atmos. Sci.*, **50**, 3477–3503.

Latif, M., and T. P. Barnett, 1995: Interactions of tropical oceans. *J. Climate*, **8**, 952–964.

—, A. Sterl, E. Maier-Reimer, and M. M. Junge, 1993: Climate variability in a coupled GCM. Part I: The tropical Pacific. *J. Climate*, **6**, 5–21.

- Lau, N.-C., S. G. H. Philander, and M. J. Nath, 1992: Simulation of ENSO-like phenomena with a low-resolution coupled GCM of the global ocean and atmosphere. *J. Climate*, **5**, 284–307.
- Legates, D. R., and C. J. Willmont, 1990: Mean seasonal and spatial variability in gage-collected, global precipitation. *Int. J. Climatol.*, **10**, 111–127.
- Levitus, S., 1982: *Climatological Atlas of the World Ocean*. NOAA Prof. Paper 13, U.S. Govt. Printing Office, 173 pp.
- Lindzen, R. S., and S. Nigam, 1987: On the role of sea surface temperature gradients in forcing low-level winds and convergence in the tropics. *J. Atmos. Sci.*, **44**, 2418–2436.
- Meehl, G. A., 1987: The annual cycle and interannual variability in the tropical Pacific and Indian Ocean regions. *Mon. Wea. Rev.*, **115**, 27–50.
- , 1990: Seasonal cycle forcing of El Niño–Southern Oscillation in a global coupled ocean–atmosphere GCM. *J. Climate*, **3**, 72–98.
- , 1993: A coupled air–sea biennial mechanism in the tropical Indian and Pacific regions: Role of the ocean. *J. Climate*, **6**, 31–41.
- Miller, R. L., and A. D. DelGenio, 1994: Tropical cloud feedbacks and natural variability of climate. *J. Climate*, **7**, 1388–1402.
- Neelin, J. D., 1991: The slow sea surface temperature mode and the fast-wave limit: Analytic theory for tropical interannual oscillations and experiments in a hybrid coupled model. *J. Atmos. Sci.*, **48**, 584–606.
- , and F.-F. Jin, 1993: Modes of interannual tropical ocean–atmosphere interaction—A unified view. Part II: Analytical results in the weak-coupling limit. *J. Atmos. Sci.*, **50**, 3504–3522.
- , I. M. Held, and K. H. Cook, 1987: Evaporation–wind feedback and low-frequency variability in the tropical atmosphere. *J. Atmos. Sci.*, **44**, 2341–2348.
- , and Coauthors, 1992: Tropical air–sea interaction in general circulation models. *Climate Dyn.*, **7**, 73–104.
- Nicholls, N., 1978: Air–sea interaction and the quasi-biennial oscillation. *Mon. Wea. Rev.*, **106**, 1505–1508.
- Philander, S. G. H., 1990: *El Niño, La Niña, and the Southern Oscillation*. Academic Press, 289 pp.
- , and R. C. Pacanowski, 1981: The oceanic response to cross-equatorial winds (with application to coastal upwelling in low latitudes). *Tellus*, **33**, 201–210.
- , N.-C. Lau, and M. J. Nath, 1992: Simulation of ENSO with a global atmospheric GCM coupled to a high-resolution tropical Pacific ocean GCM. *J. Climate*, **5**, 308–329.
- Rasmusson, E. M., and T. C. Carpenter, 1982: Variations in tropical sea surface temperature and surface winds fields associated with the Southern Oscillation/El Niño. *Mon. Wea. Rev.*, **110**, 354–384.
- Sarachik, E. S., 1974: The tropical mixed layer and cumulus parameterization. *J. Atmos. Sci.*, **31**, 2225–2230.
- Schopf, P. S., and M. J. Suarez, 1990: Ocean wave dynamics and the time scale of ENSO. *J. Phys. Oceanogr.*, **20**, 629–645.
- Seager, R., 1989: Modeling tropical Pacific sea surface temperature: 1970–1987. *J. Phys. Oceanogr.*, **19**, 419–434.
- Stommel, H., 1960: Wind-drift near the equator. *Deep-Sea Res.*, **6**, 298–302.
- Suarez, M. J., and P. S. Schopf, 1988: A delayed action oscillator for ENSO. *J. Atmos. Sci.*, **45**, 3283–3287.
- Tett, S., 1995: Simulation of El Niño–Southern Oscillation-like variability in a global AOGCM and its response to CO₂ increase. *J. Climate*, **8**, 1473–1502.
- Villwock, A., and M. Latif, 1996: Indian Ocean Response to ENSO. *J. Climate*, in press.
- Wakata, Y., and E. S. Sarachik, 1991: Unstable coupled atmosphere–ocean basin modes in the presence of a spatially varying basic state. *J. Atmos. Sci.*, **48**, 2060–2077.
- Waliser, D. E., B. Blanke, J. D. Neelin, and C. Gautier, 1994: Short-wave feedbacks and El Niño–Southern Oscillation: Forced ocean and coupled ocean–atmosphere experiments. *J. Geophys. Res.*, **99**, 25 109–25 125.
- Weare, B. C., 1983: Interannual variation in net heating at the surface of the tropical Pacific Ocean. *J. Phys. Oceanogr.*, **13**, 873–885.
- Wyrtki, K., 1975: El Niño—The dynamic response of the equatorial Pacific Ocean to atmospheric forcing. *J. Phys. Oceanogr.*, **5**, 572–584.
- Xie, S.-P., and G. H. Philander, 1994: A coupled ocean–atmosphere model of relevance to the ITCZ in the eastern Pacific. *Tellus*, **46**, 340–350.
- , A. Kubokawa, and K. Hanawa, 1993: Evaporation–wind feedback and the organizing of tropical convection on the planetary scale. Part I: Quasi-linear instability. *J. Atmos. Sci.*, **50**, 3873–3883.
- Zebiak, S. E., 1982: A simple atmospheric model of relevance to ENSO. *J. Atmos. Sci.*, **39**, 2017–2027.
- , 1986: Atmospheric convergence feedback in a simple model for ENSO. *Mon. Wea. Rev.*, **114**, 1263–1271.
- , and M. A. Cane, 1987: A model El Niño/Southern Oscillation. *Mon. Wea. Rev.*, **115**, 2262–2278.
- Zhang, C., 1993: Large-scale variability of atmospheric deep convection in relation to sea surface temperature in the tropics. *J. Climate*, **6**, 1898–1913.